The Diagnostic Value of Multi Ultra High-b-value DWI for Alzheimer's Disease

Tianxiu Zheng
Ningde Hospital Affiliated to Ningde Normal University
Qiuyan Chen
Ningde Hospital Affiliated to Ningde Normal University
Yanhua Qiu
Fujian Medical University
Deyong Zhang
Ningde Hospital Affiliated to Ningde Normal University
Liwei Shi
Ningde Hospital Affiliated to Ningde Normal University
Dingtai Wei (wdtai83@163.com)
Ningde Hospital Affiliated to Ningde Normal University

Research Article

Keywords: Alzheimer's disease, UHBV-DWI, WMH, hippocampal volume

Posted Date: August 31st, 2021

DOI: https://doi.org/10.21203/rs.3.rs-842472/v1

Abstract

To evaluate the diagnostic value of multi-ultra high b-value diffusion-weighted imaging (UHBV-DWI) in Alzheimer's disease (AD), and to build a regression prediction modelfor AD.90 participants including 30 AD, 30 mild cognitive impairments (MCI) and 30 volunteers without neurological diseases were enrolled to perform with hippocampal volume, white matter hyperintensities volume (WMH volume), periventricular white matter hyperintensity (PVWMH) score, deep white matter hyperintensity (DWMH) score and UHBV-DWI.We found UHBV-DWI outperformed in the diagnosis of AD (AUC = 0.858), and multiple linear regression model: y = 0.515 + 0.018 *(WMH volume) + 0.221 *(ADC_{uh} value)-0.359 *(left hippocampus volume) were established.So we came to a conclusion: UHBV-DWI is helpful for diagnosing AD, and the combination of WMH volume and left hippocampus volume has a better diagnostic performance.

Introduction

Alzheimer's disease (AD) is the most common neurodegenerative disease with hidden onset [1]. Clinically, it is characterized by dementia. Currently, the etiology of this condition still has not been clarified [2]. The early diagnosis of AD is of great clinical relevance, as patients with AD can benefit from early treatment and rehabilitation, especially before the occurrence of brain injury [3]. At present, the diagnosis of AD mainly relies on comprehensive evaluation of patient history, mini-mental state examination (MMSE) or neuropsychological tests by highly skilled neurologists in addition to routine MRI sequence[4, 5]. Regardless, clinical pathological studies suggested that the sensitivity and specificity of AD diagnosis by clinicians were only 70.9%-87.3% and 44.3%-70.8%, respectively [6]. Therefore, there is an urgent need to explore more robust and integrated clinical diagnostic methods that can facilitate the early diagnosis of AD.

Abnormal deposition of Aβ is an important pathological change in the occurrence and development of AD[7–9]. In recent years, AQP proteins have received increasing attention in AD research. Aquaporins (AQPs) are carriers of water molecules that Agre et al. [10] found on the cell membrane in 1993. The occurrence and development of many diseases are closely related to the expression level and distribution of AQPs and are key molecular targets in the process of diseases. Previous studies have shown that AQP proteins are involved in the transmembrane transport of water molecules, which is widely present in mammals and has 13 subtypes, namely, AQP0-12[11]. A β in the brain can be cleared by water transport, and the lack of AQPs reduces the clearance of soluble A β.[12] Studies have shown that the expression and distribution of AQPs are altered in clinical and animal models of AD.[13, 14]

The transmembrane transport of water has an important role in maintaining liquid balance between different regions, environmental steady state, and normal metabolism. Relative to conventional MR, diffusion weighted MR imaging (DWI) is the only noninvasive method that can detect water molecules in living tissue[15]. Recently, UHBV-DWI has been shown to improve the diagnostic performance of DWI in

the detection of prostate cancer and high-grade gliomas[16, 17]. Yamasaki F confirmed that UHBV-DWI could more accurately reflect cell density than conventional regular b-value DWI, but single high b-value DWI was also not accurate[17]. ADC_{uh} could eliminate the effects of microvascular perfusion and signal intensity changes, which are mainly caused by slow diffusion components[18]. Mukherjee et al. [19] confirmed that AQPs can be used as a reporter gene of the DWI-MR sequence, and the overexpression of AQPs can increase the diffusvity of water, thus resulting in signal differences detected in MRI. There is also evidence that ADC_{uh} reflects the transport of aquaporins, which might be related to the expression level of AQP4. Compared with ADC[18, 20], ADC_{uh} was more sensitive to white matter degeneration in AD[21]. UHBV-DWI molecular imaging obtains diffusion information of water molecules in microcirculation perfusion, free diffusion, and active transport of AQPs by collecting multiple DWI images with continuous b values (including low, medium and high b values) [19, 22]. An increasing number of studies have confirmed that the expression of AQPs is related to AD[23, 24], so we speculated whether UHBV-DWI can be used to diagnose AD.

In this study, we diagnosed AD and mild cognitive impairment (MCI)[25] according to medical history, the Mini-Mental State Examination (MMSE), which is widely used to screen for cognitive impairment and estimate dementia severity[26] and MRI, and selected healthy individuals without neurological diseases as controls. The diagnostic value of UHBV-DWI for AD was determined by comparison among MMSE, hippocampal volume, white matter hyperintensity volume (WMH volume)[27], periventricular white matter hyperintensity (PVWMH) score, deep white matter hyperintensity (DWMH) score and ADC_{uh} value.

Materials And Methods

Patients

This prospective study was approved by the Ningde Hospital Medical Ethics Committee affiliated with Ningde Normal University.A total of 30 patients with Alzheimer's disease who were hospitalized and clinically diagnosed in our hospital from January 2018 to December 2019 were included as the AD group; 30 patients with mild cognitive impairment and 30 healthy individuals without any neurological disease were selected as the MCI and control groups. Three groups of patients with sex, age, education time and other clinical data were not statistically significant ($p > 0.05$). Specific inclusion criteria were as follows: patients in the AD group met the diagnostic criteria of Alzheimer's disease revised in the fourth edition of the American Manual of Mental Disease Diagnosis and Statistics, and the MMSE score was less than 24 points. Patients with MCI met the following criteria: 1) awareness of subjective cognitive decline in one year; 2) MMSE score greater than 24 points; 3) Montreal cognitive assessment less than 26 points; and 4) daily life ability scale less than 26 points. The informed consent was obtained from all subjects and from a parent and/or legal guardian as Vulnerable population in the studya, all methods were performed in accordance with the principles of the 1983 Declaration of Helsinki.

MR scanning

All MR images were obtained from a 3.0-T MR scanner (General Electric, Milwaukee, WI, USA) [28]. The imaging protocol included axial three-dimensional brain volume imaging (3D T1WI), axial fast spin-echo (FSE) T2-weighted imaging (T2WI), axial T2 fluid attenuation inversion recovery (T2 FLAIR), and two SE echo-planar DWI sequences (TR msec/TE msec/excitations, 3,000/96/1; 23 sections; bandwidth, 250 kHz; section thickness, 3.0 mm; intersection gap, 0.3 mm; field of view, 240 mm×240 mm; matrix, 128×128; voxel resolution, 0.938×0.938×3.0 mm) applied in three or thogonal directions[16, 29]. The first DWI sequence was performed with standard b-values (0, 1,000 s/mm^2), while the second DWI sequence was performed with 15 different b-values (0, 30, 50, 100, 200, 300, 500, 800, 1,000, 1, 500, 2,000, 3,000, 3,500, 4,000, and 5,000 s/mm^2) [16, 30]. Eddy current correction was applied with real-time field adjustment and real-time correction of motion-induced phase error to obtain high-quality diffusion images. Spatial coverage for both DWI sequences was identical, from the lower margin of the pons to the upper margin of basal ganglia. The scan times for the sequence with standard b-values and the sequence with 15 b-values were 0.37 min and 6.85 min, respectively[20]. The total scan time of the whole examination was approximately 14 min. Head pads were used to constrain head movement in both PD patients and control subjects.

WMH volume calculation

WMH volume was calculated using the AccuBrainTM analysis system (Shenzhen Bonao Medical Technology Co., Ltd., Hong Kong, China). AccuBrainTM is a new automatic quantitative measurement tool for brain structure. The DICOM format data of 3D T1 and T2 FLAIR of all patients were compressed into Zip format files and uploaded to the AccuBrainTM cloud system for image analysis. The template is then registered with the patient image in a nonrigid manner. After registration, the predefined tags in the map are transformed and fused to generate the segmentation tags of the patient, and the volume of each tag area is recorded. After approximately 25 minutes of processing, the system will automatically generate a PDF report containing patient information, brain volume and WMH volume information. This study included the absolute volume of WMHs and the relative volume of WMHs in the PDF report (the percentage of absolute volume of WMHs in total intracranial volume) for analyses.

Grading of WMH on MRI

On the basis of the Fazekas scale[31], WMHs were visually scored using FLAIR images in the periventricular and deep subcortical areas by one of the authors, who was blinded to the patient's cognitive status. The intrarater reliability was represented with ICCs of 0.972 and 0.964 in the periventricular and deep subcortical areas, respectively. The severity of WMH in the periventricular area (PVWMH) was graded as follows: 0, no lesion; 1, cap or pencil-thin lining; 2, small halo; 3, irregular periventricular WMH extending into deep white matter. The severity of WMH in the deep subcortical area

(DWMH) was graded as follows: 0, no lesion; 1, punctate lesion; 2, beginning confluence of lesion; 3, large confluence of lesion. Figure 2E demonstrates different grades of WMH in the periventricular and deep subcortical areas. Patients were defined as having WMH if there were any identifiable WMH regardless of severity or location (either grade of PVWMH≥1 or grade of DWMH≥1). Patients were defined to have PVWMH and DWMH if graded with any nonzero grade on the region-specific Fazekas scale (PVWMH or DWMH) regardless of severity.

Quantitative image analysis

All DWI data were transferred to a GE Advanced Workstation 4.4. UHBV-DWI software in GE Functool 9.4.05a was used to perform UHBV-DWI analysis.

The ADC map was calculated from the DWI sequence using the monoexponential model by fitting b values (0, 1000 s mm−2) to equation (1)[21]

$$\frac{S}{S_0} = \exp(-b \cdot ADC) \qquad (1)$$

UHBV-ADC is calculated by fitting the five UHBVs (2000, 2500, 3000, 3500, 4000 and 4500 s/mm^2) to equation (2)[20]

$$\frac{S}{S_0} = \exp(-b \cdot ADC), b \geq \frac{\sec}{mm^2} \qquad (2)$$

T2 FLAIR was used to show the basic features of white matter hyperintensities, which were used to determine the ROI. ROIs were manually drawn on white matter hyperintensities with supporting workstation processing software, avoiding necrotic, cystic, or hemorrhagic components and adjacent normal brain tissue. The ROIs were drawn on one conventional image and automatically marked on UHBV-DWI (ADC_{uh}) and DWI (ADC) images by UHBV-DWI software in GE Functool 9.4.05a in GE Advanced Workstation 4.4, and the corresponding area of the opposite side was drawn through the mirror image. The final ADC_{uh} value represented the ROI of the overloading side/the ROI of the opposite side mirror (%).

Two experienced independent radiologists, who were blinded to the AQP results, performed ROI selection and measured each parameter value three times based on the criterion for the selection of ROIs, followed by calculating the total mean standard deviation.

Establishment and Test of Multiple Linear Regression Analysis Model

Through tidyverse, lattice, ggplot2 and caret package statistical analysis and drawing pictures. According to the independent variable to have a linear relationship with the dependent variable, the residuals are basically normally distributed. The residual variance is basically unchanged (homogeneity of variance). The residuals (samples) are independently correlated to test the model [32].

Statistical analysis

SPSS 22.0 statistical software was used for analysis. Continuous variables with a normal distribution are expressed as the mean ± standard deviation, and one-way analysis of variance was used. The classification variables are represented by percentages and tested by the $\chi 2$ test. The correlation of MRI results with AD was analyzed by Pearson correlation analysis. $P < 0.05$ was considered statistically significant.

Result

Clinical information

Thirty patients with AD, 30 patients with MCI and 30 healthy volunteers without neurological diseases (NCs) were enrolled. There were 15 males and 15 females in the AD group with a mean age of 71.23 ± 4.72 years old (range: 58–87 years old). Their mean education time was 7.89 ± 2.58 years (range: 0–13 years), and the average MMSE score was 13.1 ± 3.5. There were 13 males and 17 females in the MCI group. They were 57–85 years old with a mean age of 71.03 ± 4.85 years old. Their education time was 1–13 years with a mean education years of 8.11 ± 2.64 years, and their mean MMSE score was 24.4 ± 1.3. NC included 15 males and 15 females. Their mean age and education time were 70.73 ± 5.18 years old (range: 55–86 years old) and 7.77 ± 2.56 years (range: 1.5–15 years), respectively. In addition, their mean MMSE score was (29.1 ± 0.7). There were significant differences in MMSE scores among the three groups. Through logistic regression analysis, hypertension may be an independent risk factor for AD, while there was no significant difference in sex, age, education duration or other clinical data (Table 1, Figure 1).

Table 1

Demographic characteristics of the study participants.

Characteristics	CTL(N=30)	MCI(N=30)	AD(N=30)
Age (years)	70.73±5.18	71.03±4.85	71.23±4.72
Gender			
male	15(50%)	13(43%)	16(53%)
female	15(50%)	17(57%)	14(47%)
Weight	21.89±1.31	22.18±1.11	21.98±1.26
Education Years	7.77±2.56	8.11±2.64	7.89±2.58
Hypertension			
Yes	10(33%)	15(50%)	21(70%)
No	20(67%)	15(50%)	9(30%)
Hyperlipemia			
Yes	12(40%)	13(43%)	11(37%)
No	18(60%)	17(57%)	19(63%)
Diabetes			
Yes	8(27%)	8(27%)	7(23%)
No	22(73%)	22(73%)	23(7%7)
Smoking			
Yes	8(27%)	7(23%)	11(37%)
No	22(73%)	23(77%)	19(63%)
Drinking			
Yes	11(37%)	10(33%)	13(43%)
No	19(63%)	20(67%)	17(57%)

Hippocampal volume, MH volume, PVWMH score, DWMH score and ADC_{uh} values

At present, there are many methods for the detection of AD, such as the detection of hippocampal volume, WMH volume, PVWMH and DWMH in patients with MRI [33]. Hippocampal volume, WMH volume, PVWMH, DWMH scores and ADC_{uh} values were detected in AD patients, MCI patients and healthy volunteers. Through the composite images, we can see the contour of the hippocampus of AD, MCI, and NC, and the volume of the hippocampus of AD patients was smaller than that of MCI and NC (Figure 2A).

In addition, the high signal area of white matter was highlighted, as shown in red (Figure 2C), for analysis and calculation to facilitate the calculation of the volume of the high signal area. DWMH and PVWMH scores were positively correlated with WMH volume (figure 2E). Compared with conventional T2 FLAIR and diffusion weighted imaging (DWI) at a standard b-value (b = 1000 sec/mm^2), ADC_{uh} can show not only the signal changes in the high-signal areas of white matter but also the signal changes in the surrounding areas. By observing the three groups of $ADC_{uh,}$ we can see that the high signal area of white matter in the brain was higher, and the corresponding signal was different from that of the surrounding normal white matter (Figure 2G). There were significant differences in hippocampal volume, WMH volume, PVWMH, DWMH scores and ADC_{uh} values among 30 AD patients, MCI patients and healthy volunteers (Figure 2B, D, H, F).

Sensitivity and specificity determination

We further analyzed the sensitivity and specificity of various detection methods by ROC curve analysis. We found that ADC_{uh} had the highest value in the diagnosis of AD (AUC = 0.858), followed by WMH volume (AUC = 0.832, Figure 3A). Among them, ADC_{uh} was most sensitive in distinguishing AD from MCI (AUC = 0.802, Figure 3B), while the WMH volume was most sensitive in distinguishing AD from NC (AUC = 0.987), followed by ADC_{uh} (AUC = 0.914, Figure 3C). We found that the sensitivity of combining ADC_{uh} values and WMH volume exceeded that of a single indicator (Figure 3D). Therefore,UHBV-DWI may be used for auxiliary diagnosis of AD.

Multiple linear regression model

All-subset regression[34] showed that the left hippocampus volume, WMH volume and ADC_{uh} values could be used to jointly predict AD (Figure 4A), and a multiple regression model y = 0.515 + 0.018 *(WMH volume) + 0.221 *(ADC_{uh} value)-0.359 *(left hippocampus volume)(table 2) was established. Furthermore, we verify the established regression model. By comparing the relationship between the residual and the estimated value, it is found that they are basically independent, indicating a good linear correlation (Figure 4B). Through a normal QQ plot, we found a linear distribution of the scatter path, indicating that the residual is in line with a normal distribution (Figure 4C). The scale location diagram shows that the variance is basically a constant (Figure 4D), but residuals vs leverage confirms an extreme value with a cook distance greater than 0.5 (Figure 4E). In summary, the model can be used to diagnose AD.

Table 2

multiple linear regression model

Model	Unstandardized Coefficients		standardized Coefficients	T	P value
	B		Beta		
constant	0.515	0.267		1.928	0.057
Hippocampal（L+R）	0.070	0.070	0.161	0.994	0.323
Hippocampal(L)	-0.359	0.158	-0.435	-2.270	0.026
Hippocampal(R)	-0.032	0.150	-0.041	-0.212	0.833
WMH volume	0.018	0.008	0.214	2.210	0.030
PVWMH	0.053	0.046	0.118	1.154	0.252
DWMH	0.022	0.032	0.056	0.680	0.498
AQP-ADC	0.221	0.092	0.261	2.405	0.018

Discussion

Through the commonly used AD detection methods and UHBV-DWI for AD, MCI, and NC, we found that UHBV-DWI was highly sensitive in the diagnosis of AD patients, especially the distinction between AD and MCI. Therefore, we believe that UHBV-DWI has the potential to assist in the clinical diagnosis of AD. In addition, according to the current common AD detection methods, we established a prediction model by multiple linear regression analysis and tested the model, which is expected to diagnose AD more accurately by UHBV-DWI combined with hippocampal volume and WMH volume. At present, the main diagnostic methods of AD at home and abroad are combined with the patient's medical history, neuropsychological tests and MRI to comprehensively diagnose AD[5]. Among them, the diagnostic methods of MRI include brain hippocampus volume, WMH volume, PVWMH and DWMH. However, current studies have shown that the specificity and sensitivity of hippocampal volume, WMH volume, PVWMH and DWMH are not ideal[5, 35–37]. UHBV-DWI is currently mainly used in studies such as cerebral ischemia and Parkinson's disease, but it is not involved in AD [20, 38]. Studies have shown that AQP is abnormally expressed in the brain tissue of AD patients [39] and is associated with the expression of key proteins tau and amyloid-β in AD [40, 41], so we speculate that UHBV-DWI can be used for the diagnosis of AD. In this study, by comparing a variety of AD test methods, we proposed the guess of UHBV-DWI for AD diagnosis. By comparing a variety of AD detection methods, we not only analyzed the sensitivity and specificity of each detection method but also comprehensively analyzed the most valuable diagnostic methods and designed a prediction model. However, the number of AD, MCI and NC patients in this experiment was too small, and the designed prediction model was not verified by new experimental objects, which needs to be compensated and corrected in later experiments. Based on the above experimental analysis, we believe that UHBV-DWI has auxiliary diagnostic value for AD, but whether AQP family genes or AQP proteins have an impact on the occurrence and development of AD and whether AQP content in human blood or cerebrospinal fluid also has diagnostic value for AD are questions worthy of discussion. In the later stage,

we hope to further verify the value of UHBV-DWI by expanding the sample size and to further study the effect of AQP on the mechanism of AD to explore the role of the AQP family in the occurrence and development of AD.

Declarations

AUTHOR CONTRIBUTION

This manuscript was written by Tianxiu Zheng, data collection was completed by Tianxiu Zheng, Deyong Zhang, Yanhua Qiu and Liwei Shi, data statistics were completed by Tianxiu Zheng and Qiuyan Chen, and the subject was completed under the guidance of Dingtai Wei. All authors read and approved the final manuscript.

CONFLICT OF INTEREST

The authors declare that there are no conflicts of interest.

DATA AVAIL ABILITY

The datasets used in the project are available from the corresponding author.

ACKNOWLEDGMENTS

This work was supported by:1. Science and Technology Project of Natural Science Foundation of Fujian Province (2018J01227). 2. Medical Innovation Project of Fujian Province (2018-CXB-21). 3. Ningde Medical Technology Promotion Research Project (2020002). 4. Health Science and Technology Program of Fujian Province (2020QNA092)

References

1. Jia, J. *et al.* **Comprehensive Management of Daily Living Activities, behavioral and Psychological Symptoms, and Cognitive Function in Patients with Alzheimer's Disease: A Chinese Consensus on the Comprehensive Management of Alzheimer's Disease**. *Neuroscience bulletin* 2021.
2. Dos Santos Picanco, L. *et al.* **Alzheimer's Disease: A Review from the Pathophysiology to Diagnosis, New Perspectives for Pharmacological Treatment**. In: *Current medicinal chemistry*, 2018. pp. 3141–3159.
3. Sperling, R. *et al.* Toward defining the preclinical stages of Alzheimer's disease: recommendations from the National Institute on Aging-Alzheimer's Association workgroups on diagnostic guidelines for

Alzheimer's disease. *Alzheimer's & dementia: the journal of the Alzheimer's Association*, **7** (3), 280–292 (2011).

4. McKhann, G. *et al.* The diagnosis of dementia due to Alzheimer's disease: recommendations from the National Institute on Aging-Alzheimer's Association workgroups on diagnostic guidelines for Alzheimer's disease. *Alzheimer's & dementia: the journal of the Alzheimer's Association*, **7** (3), 263–269 (2011).
5. Qiu, S. *et al.* Development and validation of an interpretable deep learning framework for Alzheimer's disease classification. *Brain: a journal of neurology*, **143** (6), 1920–1933 (2020).
6. Beach, T., Monsell, S., Phillips, L. & Kukull, W. Accuracy of the clinical diagnosis of Alzheimer disease at National Institute on Aging Alzheimer Disease Centers, 2005–2010. *Journal of neuropathology and experimental neurology*, **71** (4), 266–273 (2012).
7. Readhead, B. *et al.* Multiscale Analysis of Independent Alzheimer's Cohorts Finds Disruption of Molecular, Genetic, and Clinical Networks by Human Herpesvirus., **99** (1), 64–8267 (2018).
8. Kumar, D. *et al.* Amyloid-β peptide protects against microbial infection in mouse and worm models of Alzheimer's disease. *Science translational medicine*, **8** (340), 340372 (2016).
9. Amtul, Z. *et al.* The Dynamics of Impaired Blood-Brain Barrier Restoration in a Rat Model of Co-morbid Injury. *Molecular neurobiology*, **55** (10), 8071–8083 (2018).
10. Agre, P. *et al.* Aquaporin CHIP: the archetypal molecular water channel. *The American journal of physiology*, **265**, F463–476 (1993).
11. Abir-Awan, M. *et al.* **Inhibitors of Mammalian Aquaporin Water Channels**.*International journal of molecular sciences*2019; 20(7).
12. Liang, R. *et al.* Aquaporin-4 Mediates the Suppressive Effect of Lipopolysaccharide on Hippocampal Neurogenesis., **23**, 309–317 (2016).
13. Yang, J. *et al.* AQP4 Association with Amyloid Deposition and Astrocyte Pathology in the Tg-ArcSwe Mouse Model of Alzheimer's Disease. *Journal of Alzheimer's disease: JAD*, **57** (1), 157–169 (2017).
14. Hoshi, A. *et al.* Altered expression of glutamate transporter-1 and water channel protein aquaporin-4 in human temporal cortex with Alzheimer's disease. *Neuropathology and applied neurobiology*, **44** (6), 628–638 (2018).
15. Chavhan, G., Alsabban, Z. & Babyn, P. Diffusion-weighted imaging in pediatric body MR imaging: principles, technique, and emerging applications. *Radiographics: a review publication of the Radiological Society of North America, Inc*, **34** (3), E73–88 (2014).
16. Seo, H., Chang, K., Na, D., Kwon, B. & Lee, D. High b-value diffusion (b = 3000 s/mm2) MR imaging in cerebral gliomas at 3T: visual and quantitative comparisons with b = 1000 s/mm2. AJNR American journal of neuroradiology 2008; 29(3):458–463.
17. Yamasaki, F. *et al.* Advantages of high b-value diffusion-weighted imaging to diagnose pseudo-responses in patients with recurrent glioma after bevacizumab treatment. *European journal of radiology*, **81** (10), 2805–2810 (2012).

18. Le Bihan, D. *et al.* Separation of diffusion and perfusion in intravoxel incoherent motion MR imaging., **168** (2), 497–505 (1988).
19. Mukherjee, A., Wu, D., Davis, H. & Shapiro, M. Non-invasive imaging using reporter genes altering cellular water permeability. *Nature communications*, **7**, 13891 (2016).
20. Xueying, L. *et al.* Investigation of Apparent Diffusion Coefficient from Ultra-high b-Values in Parkinson's Disease. *European radiology*, **25** (9), 2593–2600 (2015).
21. Tan, Y., Zhang, H., Wang, X., Qin, J. & Wang, L. The value of multi ultra high-b-value DWI in grading cerebral astrocytomas and its association with aquaporin-4. *The British journal of radiology*, **91** (1086), 20170696 (2018).
22. Schilling, F. *et al.* MRI measurements of reporter-mediated increases in transmembrane water exchange enable detection of a gene reporter. *Nature biotechnology*, **35** (1), 75–80 (2017).
23. Valenza, M., Facchinetti, R., Steardo, L. & Scuderi, C. Altered Waste Disposal System in Aging and Alzheimer's Disease: Focus on Astrocytic Aquaporin-4. Frontiers in pharmacology 2019; 10:1656.
24. Igarashi, H., Suzuki, Y., Kwee, I. & Nakada, T. Water influx into cerebrospinal fluid is significantly reduced in senile plaque bearing transgenic mice, supporting beta-amyloid clearance hypothesis of Alzheimer's disease. *Neurological research*, **36** (12), 1094–1098 (2014).
25. Qu, Y. *et al.* **Blood Biomarkers for the Diagnosis of Amnestic Mild Cognitive Impairment and Alzheimer's Disease**: **A Systematic Review and Meta-Analysis**. *Neuroscience and biobehavioral reviews* 2021.
26. Chua, X. *et al.* Mapping modified Mini-Mental State Examination (MMSE) scores to dementia stages in a multi-ethnic Asian population. *International psychogeriatrics*, **31** (1), 147–151 (2019).
27. Graff-Radford, J. *et al.* White matter hyperintensities: relationship to amyloid and tau burden. *Brain: a journal of neurology*, **142** (8), 2483–2491 (2019).
28. Meng, Y. *et al.* MRI morphologic and clinicopathologic characteristics for predicting outcomes in patients with locally advanced rectal cancer. *Abdominal radiology (New York)*, **44** (11), 3652–3663 (2019).
29. Wang, G. *et al.* Impacts of skull stripping on construction of three-dimensional T1-weighted imaging-based brain structural network in full-term neonates. *Biomedical engineering online*, **19** (1), 41 (2020).
30. De Paepe, K. *et al.* Improving lymph node characterization in staging malignant lymphoma using first-order ADC texture analysis from whole-body diffusion-weighted MRI. *Journal of magnetic resonance imaging: JMRI*, **48** (4), 897–906 (2018).
31. Fazekas, F., Chawluk, J., Alavi, A., Hurtig, H. & Zimmerman, R. MR signal abnormalities at 1.5 T in Alzheimer's dementia and normal aging. *AJR American journal of roentgenology*, **149** (2), 351–356 (1987).
32. Kern, C., Stefan, T. & Hinrichs, J. Multiple linear regression modeling: Prediction of cheese curd dry matter during curd treatment. *Food research international (Ottawa, Ont)*, **121**, 471–478 (2019).

33. DeTure, M. & Dickson, D. The neuropathological diagnosis of Alzheimer's disease. *Molecular neurodegeneration*, **14** (1), 32 (2019).
34. Hu, D., Shu, H., Hu, H. & Xu, J. **Spatiotemporal regression Kriging to predict precipitation using time-series MODIS data**.*Cluster Computing*2017;20.
35. Whitwell, J. *et al.* Neuroimaging correlates of pathologically defined subtypes of Alzheimer's disease: a case-control study. *Lancet Neurol*, **11** (10), 868–877 (2012).
36. Frisoni, G., Fox, N., Jack, C., Scheltens, P. & Thompson, P. The clinical use of structural MRI in Alzheimer disease. *Nature reviews Neurology*, **6** (2), 67–77 (2010).
37. Harper, L., Barkhof, F., Scheltens, P., Schott, J. & Fox, N. An algorithmic approach to structural imaging in dementia. *Journal of neurology, neurosurgery, and psychiatry*, **85** (6), 692–698 (2014).
38. Lee, J. *et al.* Effect of propofol post-treatment on blood-brain barrier integrity and cerebral edema after transient cerebral ischemia in rats. *Neurochemical research*, **38** (11), 2276–2286 (2013).
39. Sadashima, S. *et al.* Accumulation of Astrocytic Aquaporin 4 and Aquaporin 1 in Prion Protein Plaques. *Journal of neuropathology and experimental neurology*, **79** (4), 419–429 (2020).
40. Park, J. *et al.* Neuronal Aquaporin 1 Inhibits Amyloidogenesis by Suppressing the Interaction Between Beta-Secretase and Amyloid Precursor Protein. *The journals of gerontology Series A, Biological sciences and medical sciences*, **76** (1), 23–31 (2021).
41. Misawa, T., Arima, K., Mizusawa, H. & Satoh, J. Close association of water channel AQP1 with amyloid-beta deposition in Alzheimer disease brains. *Acta neuropathologica*, **116** (3), 247–260 (2008).

Figures

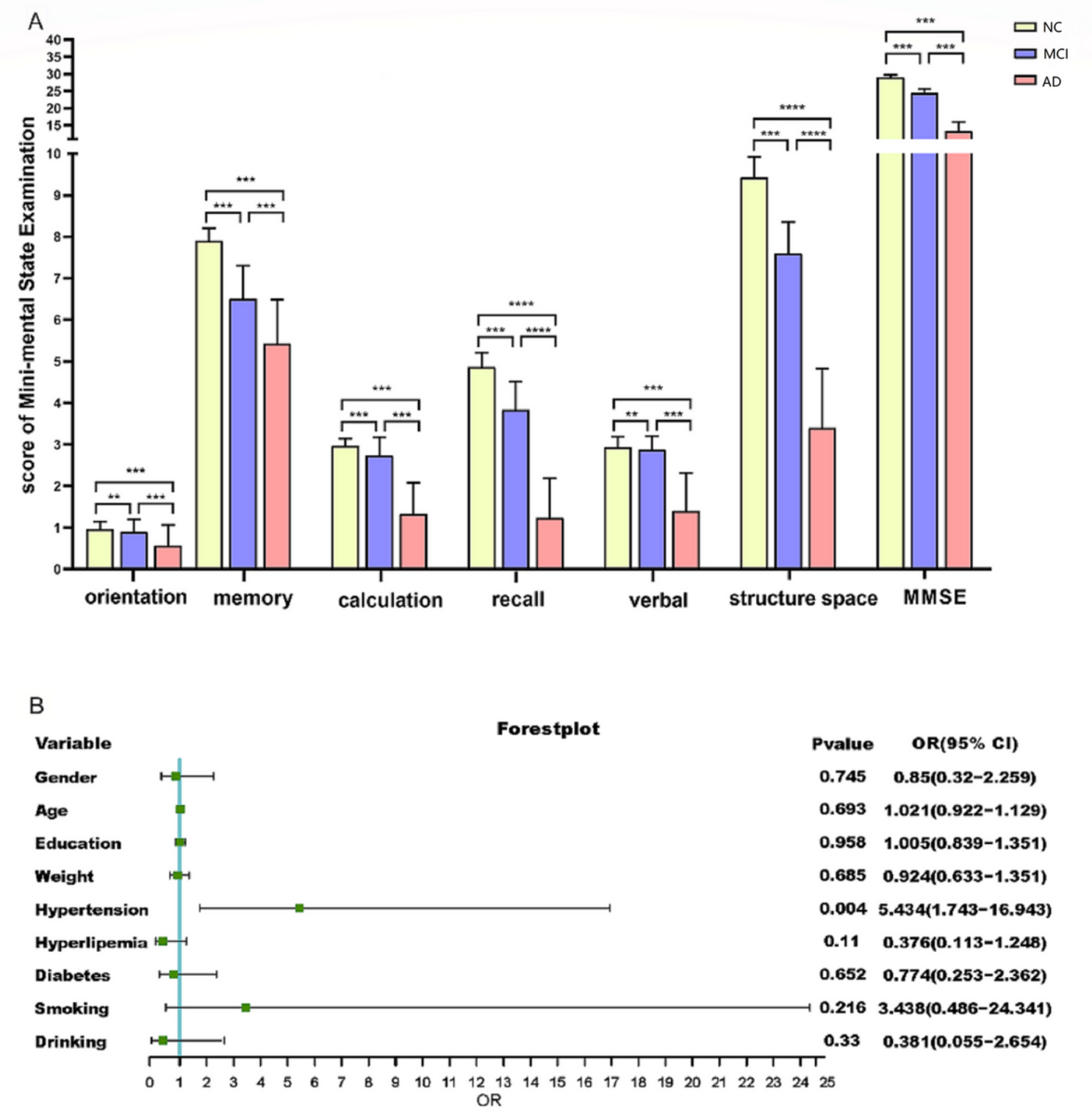

Figure 1

Clinical information: A. Neuropsychological tests included the MMSE score, orientation, memory, calculation, recall, verbal, and structure space. B. Logistics regression analysis detects the relationship between age, sex, weight, education years, hypertension, hyperlipemia, diabetes, smoking, drinking and AD.

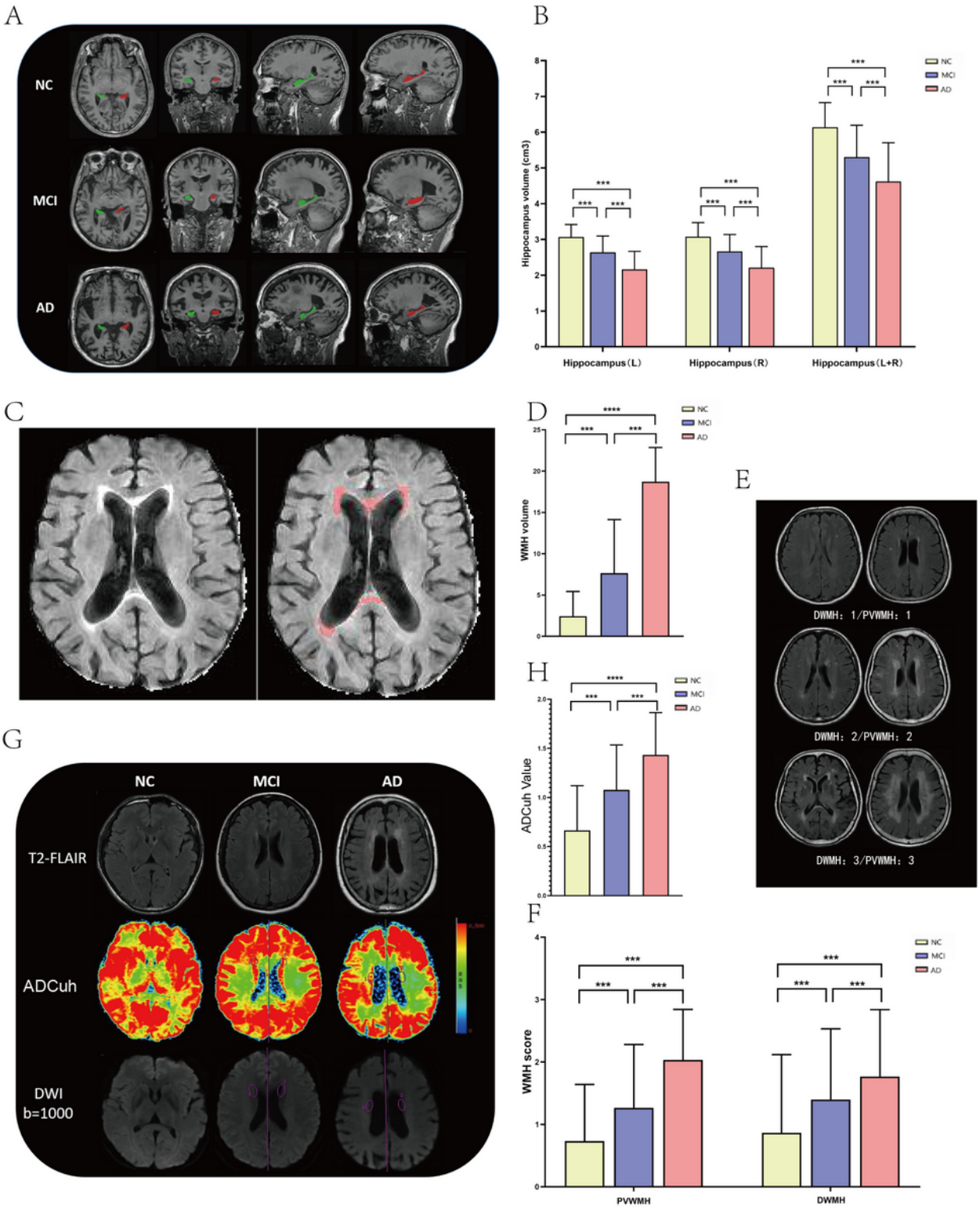

Figure 2

Hippocampal volume, WMH volume, PVWMH, DWMH scores and ADCuh values: A. Representative images of Hippocampal. The left hippocampus is represented in green, and the right hippocampus is represented in red. B. Histogram shows the volume of the hippocampus in 30 cases of AD, MCI, and NC. C. Representative images of segmentation for WMHs by AccuBrainTM. Red areas are regions of WMH after automatic segmentation by AccuBrainTM. D. Histogram shows the relative volume of white matter

high signal in 30 cases of AD, MCI, and NC. E. Representative images of the application of the Fazekas Scale. F. Histogram shows PVWMH and DWMH scores in 30 cases of AD, MCI, and NC. G. Representative images of ADCuh.H. Relative expression of ADCuh values.

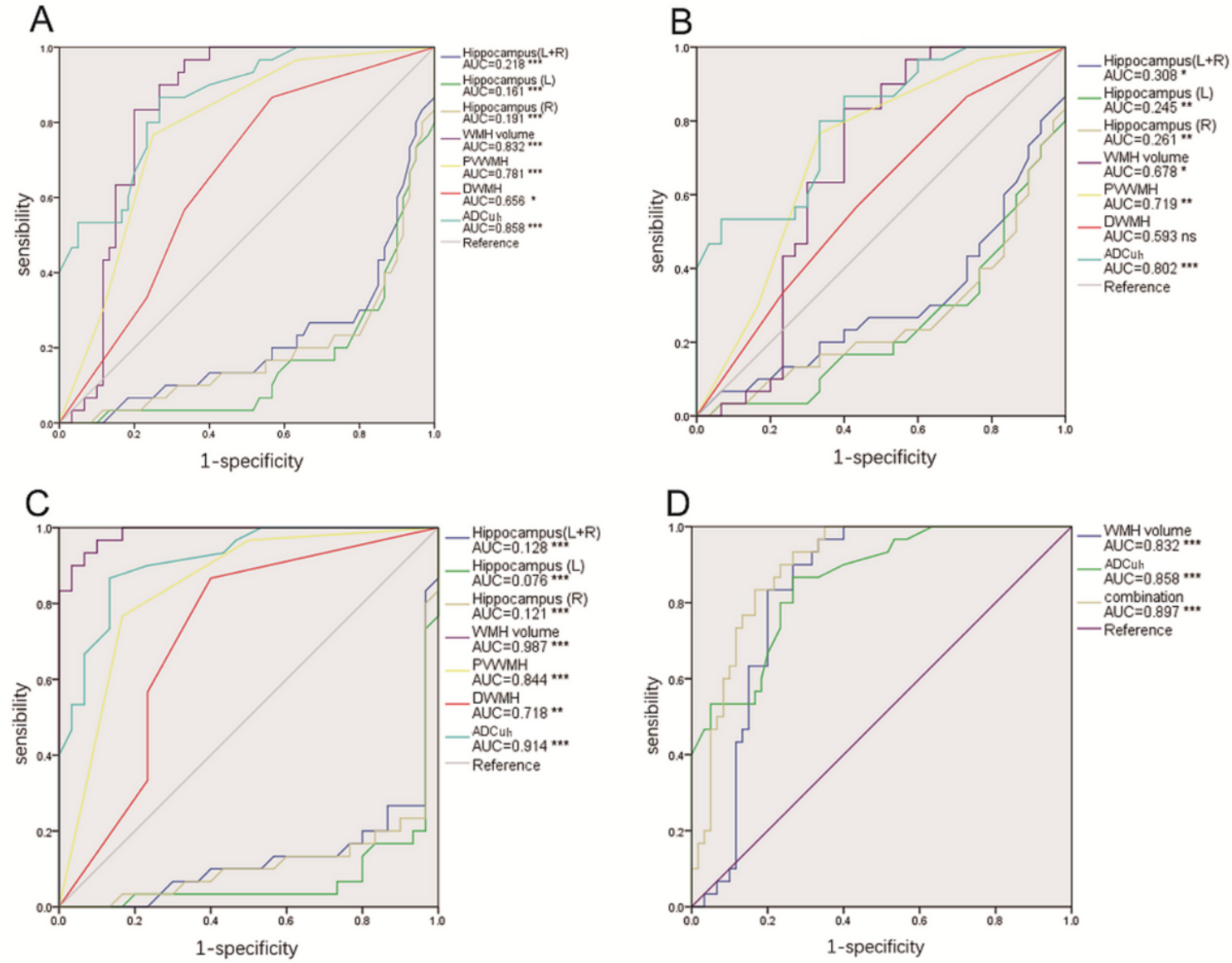

Figure 3

Sensitive and specific detection: A. ROC analysis shows the diagnostic sensitivity and specificity of hippocampal volume, WMH volume, PVWMH, DWMH scores and ADCuh values for AD. B. ROC curve shows the diagnostic sensitivity and specificity of the above methods from AD to MCI. C. ROC curve shows the diagnostic sensitivity and specificity of the above methods from AD to NC. D. Sensitivity and specificity of the combined diagnosis of WMH volume and ADCuh values.

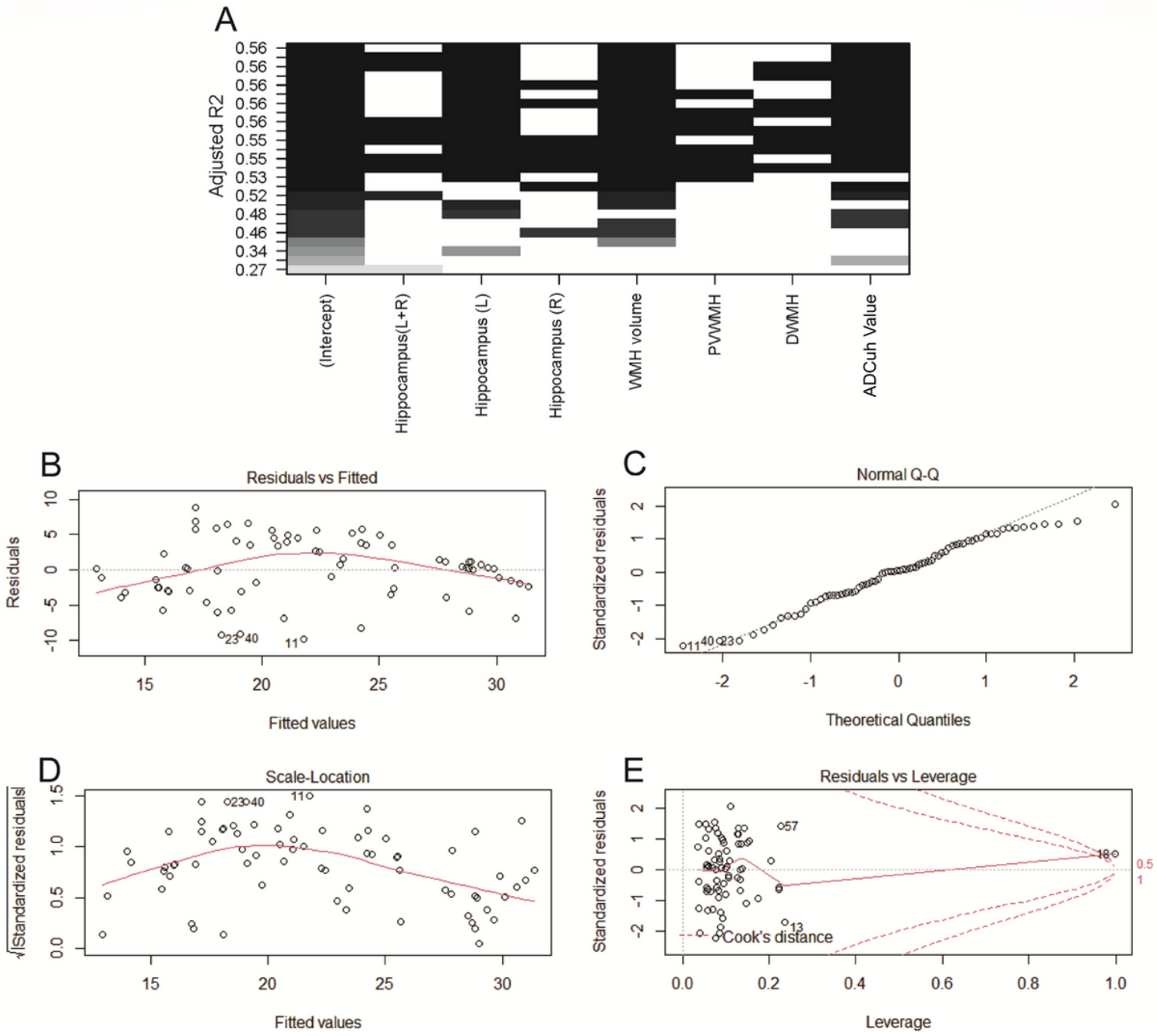

Figure 4

Multiple linear regression model: A. Full subset regression. The ordinate represents the value of Adjusted R2. B. Residual vs fitted plots show whether residuals have nonlinear patterns. equally spread residuals around a horizontal line without distinct patterns represent nonlinear relationships. C. Normal Q-Q plot if residuals are normally distributed, residuals follow a straight line well represent normally distributed. D. Scale-location plot shows whether residuals are spread equally along the ranges of predictors. horizontal line with equally (randomly) spread points represent equal variance. E. Residual vs leverage plot helps us to find influential cases and extreme values.